Design of the compact, stable vertical rice seedling frame for cold regions with DLI-based dynamic light control

Lifeng Guo[1,2,3†], Fahui Wu[2,3†], Junjie Huang[2,3], Yizhe Wang[2,3], Yujian Bao[2,3], Ziliang Li[2,3], Yuzhu Wu[2,3], Ru Tang[4], Zhongbin Su[3*], Qiuju Xie[1*], Zheng Ma[1,3], Liwei Wang[1,3], Xin Zhang[5]

(1. *College of Intelligence Science and Engineering, Northeast Agricultural University, Harbin 150030, China*;
2. *College of Agricultural Equipment and Energy Engineering, Northeast Agricultural University, Harbin 150030, China*;
3. *Key Laboratory of Northeast Smart Agricultural Technology of Ministry of Agriculture and Rural Affairs, Harbin 150030, China*;
4. *Zhejiang Cfmoto Power Co., Ltd., , Hangzhou 311103, China*;
5. *School of Mechanical Engineering, Southeast University, Jiangsu Key Laboratory for Design and Manufacturing of Precision Medicine Equipment, Nanjing 211189, China*)

Abstract: Traditional flat-bed rice nurseries in cold regions require large areas and suffer from inefficient tray movement and instability. A compact vertical rice seedling frame is developed in this work, which integrates a triangular-stabilized tray support, a four-point conveying mechanism, and anti-tilt/anti-torsion features, coupled with a dynamic lighting control strategy based on daily light integral (DLI). The mechanical design was validated by finite-element analysis under design loads, and collision-free operation was confirmed by digital mock-up simulation and prototype tests. In greenhouse trials comparing the vertical frame to conventional flat cultivation, the frame increased space-use efficiency to ΔP = 119.29% (i.e., ≈19.29% higher than the flat bench), while maintaining seedling coverage at 98%±1% (ns) and stem diameter (ns), and producing significantly shorter (more compact) seedlings (p<0.05; *a*/*b*). These results demonstrate a practical pathway for high-density automated seedling production in cold climates using intelligent vertical systems.

Keywords: vertical seedling frame, four-point conveying, anti-tilt rod, daily light integral, LED control, finite-element analysis, greenhouse experiment

DOI: 10.25165/j.ijabe.20261902.10316

Citation: Guo L F, Wu F H, Huang J J, Wang Y Z, Bao Y J, Li Z L, et al. Design of the compact, stable vertical rice seedling frame for cold regions with DLI-based dynamic light control. Int J Agric & Biol Eng, 2026; 19(2): 112–119.

1 Introduction

Rice is a staple crop whose establishment and yield are highly sensitive to the vigor and uniformity of transplants[1-3]. In cold regions, low temperature and weak winter irradiance constrain conventional nursery practices, motivating compact, automated systems that stabilize the microclimate and improve space-use efficiency[4,5]. Multilayer or vertical nursery structures can greatly increase plant density per unit floor area compared with flat benches, while providing a controllable environment for year-round seedling production.

Despite their potential, many existing nursery systems still face mechanical and operational limitations that affect reliability and growth uniformity[6,7]. Tray frames or hanging mechanisms may lack sufficient rigidity, causing tilting or jamming during circulation; misalignment and torsion in vertical chain runs further aggravate posture instability and wear[8]. In rice production, various mechanized seedling and handling solutions—from factory-style three-dimensional carpet systems to automated plate-lifting/transplanting equipment—have been explored to raise throughput, yet stability at turnarounds, anti-tilt measures, and robust conveyance remain key bottlenecks for continuous operation[9-11].

Environmental non-uniformity across tiers is another critical challenge[12]. Non-uniform photon delivery in tall racks produces layer-wise variation in morphology and biomass, especially under fixed lighting schedules. The daily light integral (DLI)—the 24 h integral of photosynthetic photon flux density (PPFD)—is a central metric linking light environment to seedling quality; both insufficient and excessive daily dose can lead to suboptimal development or photoinhibition[13-16]. In winter greenhouses, when solar DLI is consistently below cultivar targets, supplemental LED lighting is required to sustain seedling growth and uniformity. Recent ray-tracing and 3D canopy modeling studies provide a physics-based basis for sizing supplemental lighting and diagnosing

Received date: 2025-11-09 **Accepted date:** 2026-03-15

Biographies: **Lifeng Guo**, Senior Engineer, research interest: intelligent agricultural equipment, Email: guolifeng@neau.edu.cn; **Fahui Wu**, MR, research interest: intelligent agricultural machinery, Email: a07230498@neau.edu.cn; **Junjie Huang**, MR, research interest: structural reliability of intelligent equipment, Email: a07220289@neau.edu.cn; **Yizhe Wang**, MR, research interest: agricultural machinery automation, Email: a07230182@neau.edu.cn; **Yujian Bao**, MR, research interest: dynamic analysis of mechanical systems, Email: a07230185@neau.edu.cn; **Ziliang Li**, MR, research interest: agronomy-equipment adaptation, Email: a07240185@neau.edu.cn; **Yuzhu Wu**, MR, research interest: crop growth phenotypic data processing, Email: a07220052@neau.edu.cn; **Ru Tang**, Engineer, research interest: precision machining technology, Email: leontang007@hotmail.com; **Zheng Ma**, PhD, research interest: intelligent control algorithm and application, Email: zavier_ma@outlook.com; **Liwei Wang**, PhD, research interest: agricultural intelligent detection and sensing, Email: wlw199402@163.com; **Xin Zhang**, MR, research interest: structural optimization of intelligent equipment, Email: 220240346@seu.edu.cn.

†These authors contributed equally to this work.

***Corresponding author: Zhongbin Su**, Professor, research interest: agricultural electrification and automation. Key Laboratory of Northeast Smart Agricultural Technology of MARA, Harbin 150030, China. Tel: +86-13303609163, Email: suzb001@163.com; **Qiuju Xie**, Professor, research interest: agricultural electrification and automation. College of Electrical Engineering and Information, Northeast Agricultural University, Harbin 150030, China. Tel: +86-13936727953, Email: xqj197610@163.com.

tier-level light deficits in vertical structures[17].

LED technology and control make DLI-driven management practical[18]. High-efficacy horticultural LEDs, combined with spectrum-aware strategies (e.g., red: blue tuning) under a target DLI, can improve transplant quality and operational flexibility while controlling energy use[19-21]. Sensor-integrated systems with tier-mounted quantum/DLI sensing and closed-loop dimming (PI/PWM) enable hour- or day-level regulation of photon dose to equalize exposure among tiers and avoid over-lighting[22-24]. These advances, together with compact mechanical designs, motivate an integrated approach that couples a robust four-point conveying architecture and anti-torsion/anti-tilt measures with DLI-based, tier-wise feedback control[25,26]. The objective of this study is therefore to design and validate a compact, stable vertical seedling frame tailored for cold-region greenhouses and to implement an intelligent DLI control loop that delivers uniform daily photon dose across tiers while achieving a substantial increase in land-use efficiency[27-29].

2 Materials and methods

2.1 System architecture and overall design

The vertical seedling frame is a compact welded steel structure designed for high-density, modular nursery production. The rack measures approximately 2.5 m×2.5 m in floor projection and 2.6 m in height, fitting conventional greenhouses. Seedling trays circulate along the rack via a dual-chain conveying mechanism: a pair of synchronized roller chains (31.75 mm pitch, ANSI 20A) runs up one side and down the other, carrying trays in a continuous loop. A motor-gearbox at the base drives the left sprocket; torque is transferred to the right sprocket via a rigid drive shaft, ensuring synchronous motion. Tray posture is maintained by a triangular linkage support and inclined anti-tilt rods with pulleys on eccentric vertical rails, preventing tipping and interference at the sprockets. The system operates in timed stepping cycles with dwell periods for lighting and seedling management operations.

The prototype's integrated architecture comprises three subsystems: 1) a conveying mechanism (dual-chain loop, trays, anti-tilt/anti-torsion rods); 2) dimmable LED lighting arrays (horticultural spectrum) above each tier; and 3) a sensor-based control system. The conveying mechanism forms a closed loop that lifts trays along one side and lowers them on the other; the triangular supports and anti-tilt rods maintain tray orientation throughout movement. Each LED array is positioned above its tier to ensure uniform photosynthetic photon flux (PPFD) on the tray surface. The control system consists of PPFD and ambient sensors, a microcontroller (ARM-based), and motor/LED drivers.

Key design parameters were chosen for standard nursery compatibility and compactness: belt (chain) width is 200 mm, and tray pitch (560 mm center distance) matches standard tray sizes while keeping aisles narrow. The pulley-to-guide spacing was set so anti-tilt rods remain engaged throughout the run and at turnarounds, minimizing lateral play. The chain center distance (30 links, 570 mm) provides adequate wrap and tension adjustability, with pre-tension to avoid sag under full load. Preliminary checks confirmed that shafts, sprockets, and tray beams meet strength and deflection criteria under these parameters.

Figure 1a illustrates the mechanical structure of the vertical seedling cultivation frame. Figure 1b presents the DLI-based dynamic supplemental lighting control framework integrated into the system, which is not merely an auxiliary lighting function but one of the core components of the overall system design. Within this control framework, a PPFD sensor is installed on each tier to monitor the incident light intensity at tray height, and the controller integrates the measured PPFD over time to calculate the actual daily light integral, DLI_act (mol/m^2·d). The calculated DLI_act is then continuously compared with the target value set for different seedling growth stages[30]. Based on the deviation between DLI_act and DLI_set, the controller employs a dimming strategy derived from proportional-integral/proportional-integral-derivative (PI/PID) control, dynamically regulating the daily photon dose of each tier within the desired range by adjusting the LED PWM duty cycle or driving current. Meanwhile, the system coordinates the tray circulation process with the supplemental lighting schedule to ensure consistent light exposure time and cumulative light dose for each tray during circulation.

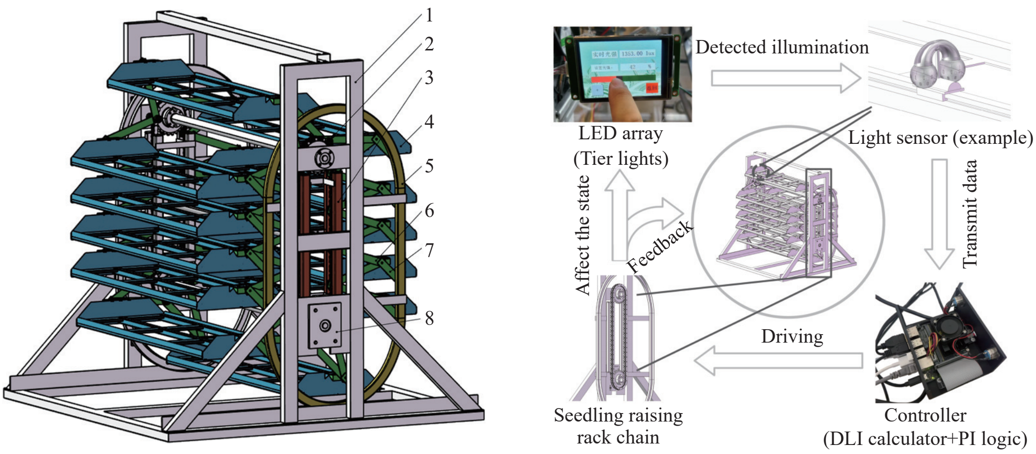

a. Structure diagram of rice seedling frame b. DLI-based closed-loop supplemental lighting control system

1. Seedling rack frame 2. Chain 3. Chain anti-torsion device 4. Seedling tray 5. Anti-tilt guiding mechanism 6. Triangular stabilized seedling tray support 7. Four-point tray conveying mechanism 8. Transmission system

Figure 1 Structure diagram of rice seedling frame and control system

To realize DLI-based dynamic supplemental lighting control in the overall design of the seedling system, each tier is equipped with a PPFD sensor (±5% accuracy) to monitor the incident light intensity at tray height, while an encoder mounted on the drive shaft provides position feedback for tray stepping and limit switches protect the end positions[31]. Temperature and humidity sensors are installed near the canopy to monitor the local microclimate, and constant-current LED drivers support PWM dimming (0-10 V or

PWM input). To reduce shock loads during tray circulation, the system adopts a DC motor driver (or AC inverter) to achieve soft-start and soft-stop control[32]. Based on these input signals, the ARM controller calculates the actual daily light integral, DLI_act, at 1 min integration intervals. Subsequently, under current and temperature constraints, a PI regulator adjusts LED intensity to reduce the deviation between DLI_act and the target value DLI_set. Meanwhile, tray stepping is coordinated with the supplemental lighting schedule to ensure that each tray receives the required photoperiod and cumulative photon dose without exceeding the daily DLI budget. The resulting integrated control loop is illustrated in Figure 1b.

The key mechanisms were designed to ensure stable tray circulation and accurate DLI delivery, including the pulley/rail offset, chain center distance, tray spacing, and LED channel sizing[33]. (a) Pulley/rail offset: set so any tray pitch generates a restoring moment at ≈45° between anti-tilt rod and vertical, minimizing force needed; (b) Chain center distance: chosen as 30 links, providing ample wrap angle and 1%-2% tensioner take-up; (c) Tray spacing: vertical spacing set by chain spacing between hinges (not tray thickness), preventing sprocket interference; (d) LED channels: sized for the highest target DLI scenario at minimum photoperiod, with 20%-30% headroom for LED aging and temperature derating.

Table 1 summarizes the target light environment requirements of rice seedlings at different growth stages, including light intensity, photoperiod, target DLI, and the red-to-blue spectral ratio. During system operation, real-time sensor data are used to measure the PPFD of each tray and calculate DLI_act. Each day, the control logic (Figure 2) compares actual DLI to the target range: if actual DLI is below the lower bound, supplemental lighting is activated; if above the upper bound, lighting is reduced; if within range, current conditions are maintained. Tray movements and lighting are coordinated so that each tray receives its prescribed DLI efficiently over each 24 h cycle. Thus, this control framework achieves consistency among the system architecture, operational methodology, and subsequent evaluation of supplemental lighting performance.

Table 1 Lighting setpoints and spectra by seedling stage used in the experiments (PPFD-based control with DLI targets)

Stage (days after sowing)	Photoperiod/ h	PPFD setpoint/ (μmol·m^{-2}·s^{-1})	Target DLI/ (mol·m^{-2}·d^{-1})	LED spectrum (R:B)	Note
Ⅰ (0–5 d) – emergence	16	160	9.2	2.0	Lower light to avoid etiolation and overheating during emergence.
Ⅱ (6–12 d) – leaf expansion	16	240	13.8	2.0	Core growth phase; DLI set as main target for uniform vigor.
Ⅲ (13–18 d) – hardening	16	200	11.5	2.0	Slightly reduced dose to promote compact, transplant-ready seedlings.

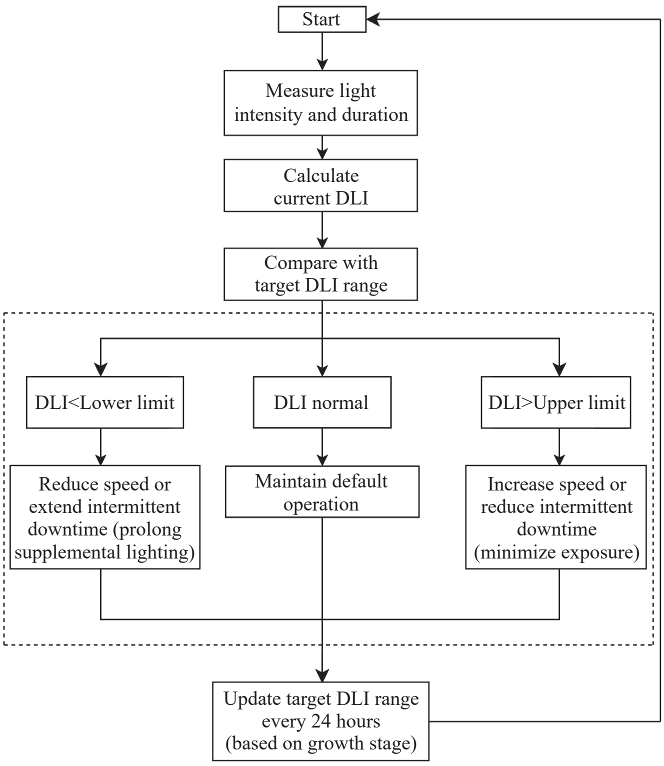

Figure 2 DLI-based control decision flowchart

2.2 Structural design of the triangular support and four-point conveying mechanism

As illustrated in Figure 3, each seedling tray is supported by an isosceles triangular linkage and an inclined anti-tilt rod engaging an eccentric vertical guide rail. Points A and B are hinges between rods and chain segments; Point C is the hinge point of the supporting and anti-tilt rods with the tray mount; Point D is the hinge between the anti-tilt rod and pulley. Four restraint points—the two chain hinges, the triangular apex, and the rod–rail contact—maintain a level posture through vertical runs and sprocket turnarounds. Two steel support rods form a rigid triangle between the moving chain and the tray base; the plane of the triangle is parallel to the chain plane, constraining tray rotation and balancing chain forces across both rods. Outward suspension at point C prevents interference at sprockets, and vertical spacing is determined by the chain link distance between hinges A and B rather than by tray thickness. The anti-tilt rods press against offset guide rails when the tray tends to tip, producing a restoring moment that stabilizes posture under uneven loads.

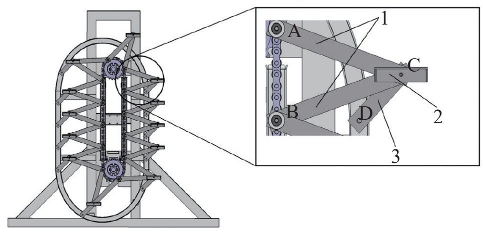

1. Supporting rod 2. Tray mounting base 3. Anti-tilt rod

Figure 3 Four-point conveying mechanism structure diagram

2.3 Design of the chain anti-torsion device

To suppress lateral drift and twist in the vertical chain legs, a chain anti-torsion device is mounted parallel to each chain (Figure 4). A longitudinal guide rail is fixed to the rack, and two low-friction pulleys mounted on a short pin on the support linkage slide along the rail. Under lateral or torsional perturbations, rail–pulley contact constrains the vertical run, re-centers the chain prior to sprocket entry, and distributes loads to limit yaw. This passive constraint improves tracking stability and reduces wear of the chain and sprockets during continuous operation.

2.4 Transmission system design

The drive system includes an electric motor, flexible coupling, gearbox, and a driven sprocket that pulls the roller chain. A 20A single-row roller chain (ANSI standard) was selected for its balance of strength and cost. A tray circulation speed of 0.06 m/s (matching the typical turnover intervals for seedling cultivation) was set as the design target, which corresponds to a sprocket speed of approximately 4.7 r/min with the selected sprocket diameter. Manufacturer data for a 20A chain indicate a continuous power rating of 0.5 kW (Figure 5).

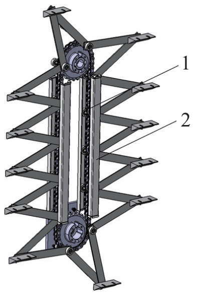

1. Anti-torsion slider 2. Longitudinal anti-torsion guide

Figure 4 Chain anti-torsion device structure

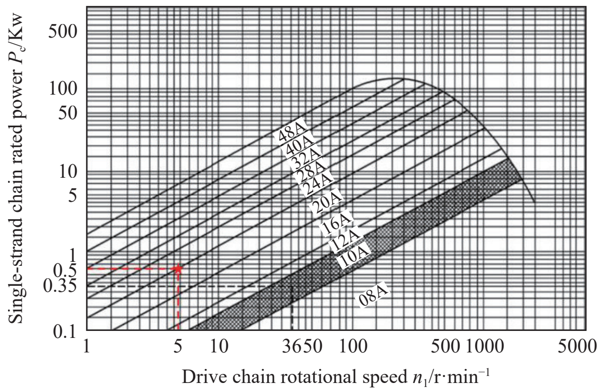

Figure 5 Rated power curve of A-series single-row roller chains

The chain capacity was checked using Equation (1):

$$P_{ca} = (K_A K_z)/K_p P \le P_c \tag{1}$$

where, P_{ca} is the calculated chain power, P is the motor power, P_c is the chain's rated power, K_A=1 (service factor), K_z=0.78 (tooth count factor), and K_p=1 (chain row factor). Substituting these yields $P\le$ 0.64 kW for the motor. To provide a margin, a 0.55 kW (YB2-712-2 series) three-phase asynchronous motor was selected, which drives the sprocket and thus the tray chain at the required speed without exceeding the chain's capacity.

2.5 Key parameter analysis

2.5.1 Parametric analysis of the anti-tilt rod

The anti-tilt guiding mechanism is idealized as a planar statics model with hinges (Figure 6) A and B on the chain, hinge C at the tray mount, and hinge D at the rod–pulley interface. Let I_{CD} be the distance CD, α the angle between CD and vertical, and β the rod angle to vertical. Moment equilibrium gives

$$T = I_{CD}\cdot 2F' = I_{CD}\cdot 2[F\sin(\alpha+\beta)] \tag{2}$$

In the limiting case $\alpha=\beta$, this simplifies to

$$T = I_{CD}\cdot 2F' = 2I_{CD}F\sin(2\alpha)\cdot(0^\circ \le \alpha \le 90^\circ) \tag{3}$$

Solving for F gives:

$$F = \frac{T}{2I_{CD}\cdot\sin(2\alpha)} \tag{4}$$

Thus F is minimized when sin (2α) is maximized; choosing α=45° minimizes the required stabilizing force for a given tipping moment.

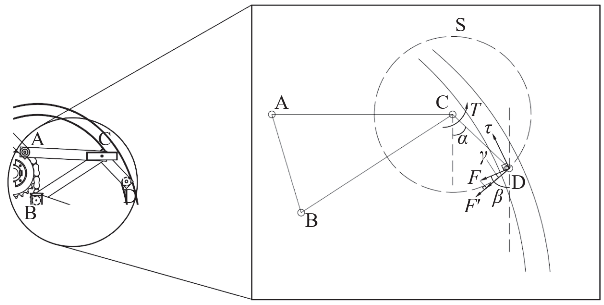

Note: A and B are hinges between rods and chains; C is the hinge between support, anti-tilt rods, and mount; D is the hinge between the anti-tilt rod and pulley. Circle S is centered at C with radius CD. Angle between CD and vertical is α; angle between support force and vertical is β.

Figure 6 Simplified anti-tip guiding mechanism and force analysis

2.5.2 Boundary condition analysis of the seedling tray

The weights of twenty fully loaded trays of commonly used types (Table 2) were measured to determine the worst-case load conditions. The maximum tray mass m_{max} determines the maximum distributed load p_{max} by

$$p_{max} = \frac{m_{max}\cdot g}{S} \tag{5}$$

where, S is tray area. Table 2 summarizes tray dimensions, masses, and calculated pressures (up to 270 Pa). For safety, a uniform load of 300 Pa (above all measured pressures) was applied in analysis. Assuming 45Cr steel trays (yield 355 MPa) with safety factor n_s=1.5, the allowable bending stress is $\sigma_{allow}\approx$236.67 MPa. Under a 300 Pa uniform load with tray ends fixed, the calculated maximum bending stress was only 8 MPa, with center deflection 0.2 mm (Table 3). These values are far below allowable limits, confirming the tray's strength and rigidity.

Table 2 Hard tray parameters

Type	Length/mm	Width/mm	Height/mm	Mass/kg	Load/Pa
Blanket hard tray	580	280	25	3.368	203.24
Pot-type hard tray	580	280	25	3.875	233.84
Pot-shaped blanket tray	580	280	25	4.486	270.71

Table 3 Material properties of the tray (45Cr steel)

Property	Numerical value
Yield strength	355 MPa
Young's modulus	2.09×10^5 MPa
Poisson's ratio	0.269
Density	7850 m^3

3 Design of key components

3.1 Design of the seedling tray

A rigid, flat-bottomed rectangular steel tray was selected for structural robustness. Typical commercial rigid trays are 580 mm×280 mm×25 mm internally. To accommodate multiple flats, the prototype tray base was enlarged to 1880 mm×660 mm (Figure 7). The tray underside features a longitudinal main beam and multiple transverse reinforcing beams (Figure 7) to increase rigidity under load. This framework ensures that applied seedling loads are carried by the steel structure without excessive deflection.

3.2 Triangular stabilized support and four-point conveying mechanism

Using Equations (2)-(5) and the worst-case T derived from Sections 2.5.1 and 2.5.2, the required stabilizing force for the selected geometry remains below the allowable for the chosen steel rods with a safety factor >2. Digital mock-up (DMU) and prototype circulation confirmed clearance at sprockets and along vertical runs; no posture loss or interference was observed. The validated kinematics are consistent with the four-point layout and triangular support shown in Figure 3, demonstrating that the 45° anti-tilt configuration provides the intended restoring moment under uneven loads.

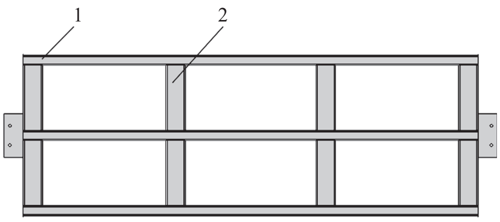

1. Beam 2. Reinforcing beam

Figure 7 Bottom structure of the tray

3.3 Chain anti-torsion device

With the guide-rail/pulley constraint engaged, vertical-leg alignment was maintained during start/stop transients, and twist-induced skew at sprocket entry was not detected. Compared with preliminary runs without the device, roller-climb events were eliminated and chain tracking stabilized, meeting the acceptance criterion of no measurable twist-induced posture error at tier entry. The device layout is shown in Figure 4.

3.4 Transmission system design

For pitch p and z=24, sprocket geometry (indexing, tip/root diameters, tooth height) follows standard formulas and is reported with the chain-drive evaluation. The capacity check in Equation (1) supports the 0.55 kW motor selection with margin for start-up transients and the heaviest tray set. Performance targets were met in prototype operation (≈0.06 m/s) without overload indications. Detailed sprocket parameters are provided in Table 4, ensuring compliant engagement under the validated load envelopes.

Table 4 Main parameters of the 24-tooth sprocket

Number of teeth z	Pitch circle diameter d/mm	Tip diameter d_a/mm	Root circle diameter d_f/mm	Tooth height h_a/mm
24	243.25	254	224.20	6.35

3.5 Key parameter analysis (numerical outcomes & sensitivity)

Applying Equations (2)-(5) with the inputs in Tables 2 and 3 yields a conservative uniform surface load and allowable-stress margin confirmed by finite element analysis (FEA). FEA results for the tray (45Cr) show maximum von Mises stress ≈8.05 MPa and deflection ≈0.201 mm—well below σ_{allow}—and chain-pin stresses remained below the allowable 236.67 MPa for 45Cr steel. Sensitivity follows F∝1/sin(2α): deviating ±15° from 45° increases the required stabilizing force by >30%, supporting the selected anti-tilt angle for robustness across operating conditions.

4 Finite element analysis results

4.1 Finite element analysis of the seedling tray

To verify the seedling tray's structural integrity, a static finite element analysis (FEA) was performed on its 3D model (CATIA). The tray is modeled in 45Cr steel; material properties are given in Table 3. The mesh used tetrahedral elements (Figure 8a). Under the 300 Pa uniform load, the maximum stress occurred at the midpoint of the main beam and side edges, and was only 8.05 MPa – far below the allowable 236.67 MPa (Figure 8b). The maximum deflection was 0.201 mm at the center of the tray (Figure 8c). These results indicate that the tray design meets rigidity and strength requirements.

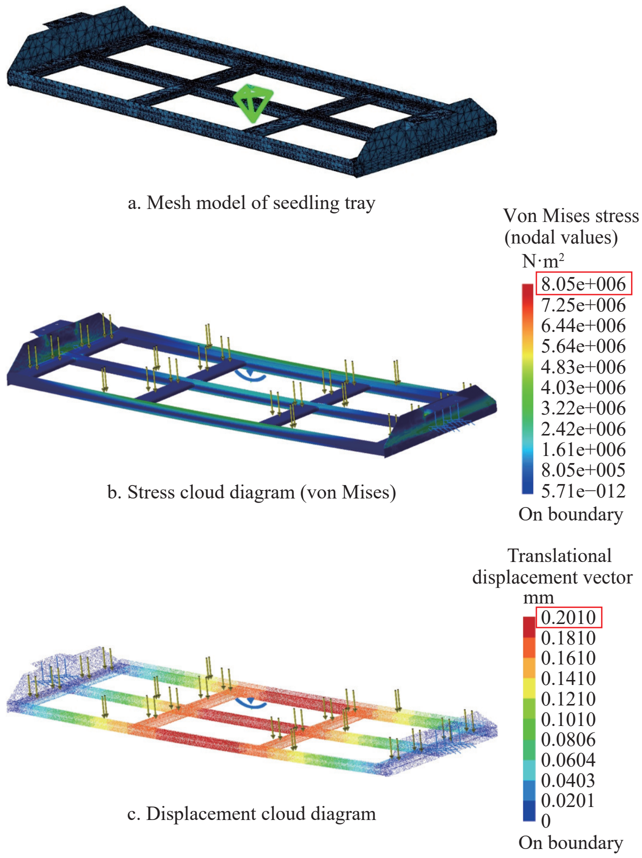

Figure 8 Static finite element analysis results of the rice seedling tray

4.2 Chain drive analysis

The tray–chain connection was analyzed by modeling the tray hinge as a simply supported beam (Figure 9). The beam supports the weight of multiple seedling trays and contents (total gravitational load G). Under a uniform mid-span load, the support reactions are F_1=F_2=G/2, so each hinge pin carries G/2. In our design, each pin carries six fully loaded trays plus the chain mass, i.e. G=(6m_1+m_2)g (where m_1= mass of one loaded tray, m_2 = mass of chain and fittings).

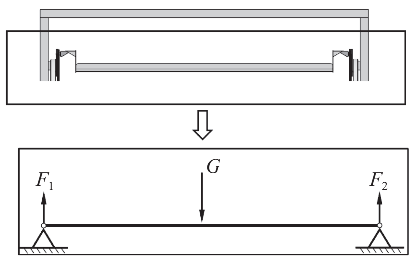

Figure 9 Simplified force model of tray-to-chain connection used for force analysis. Each support carries G/2.

For FEA, a small notch (width = 1% of pin diameter) was introduced at the load point to avoid artificial stress peaks. Figure 10 shows the von Mises stress distribution in the pin cross-section under this load. The pin (45Cr steel, allowable 236.67 MPa) saw a maximum stress below the allowable limit (Figure 11). Thus the pin design is safe for the applied load.

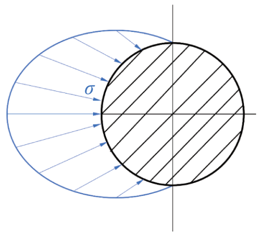

Figure 10 FEA stress distribution (cross-section view) in the pin under load

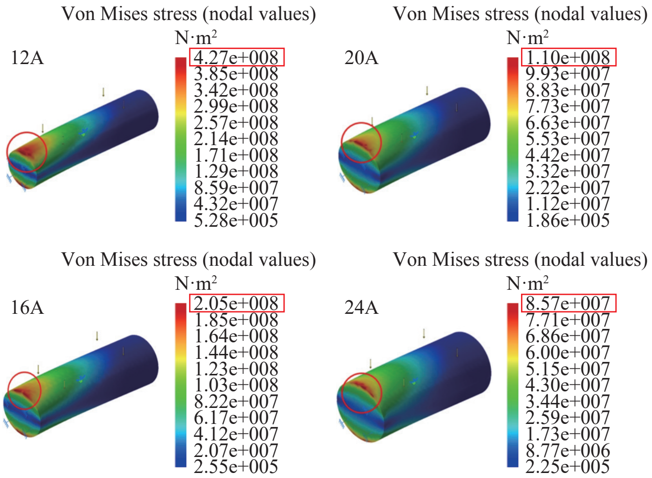

Figure 11 FEA stress cloud of the pin (45Cr steel) under the applied load; stresses remain below the allowable 236.67 MPa

The chain drive design was completed by specifying both driving and driven sprockets as 24-tooth units made of quenched steel. Using the chain pitch p=31.75 mm, roller diameter d_1= 19.0 mm, and z=24, standard sprocket geometry formulas give a pitch circle diameter d≈243.25 mm, tooth top diameter d_a≈ 254.00 mm, root diameter d_f≈224.20 mm, and tooth height h_a= 6.35 mm (Table 4). These values ensure proper chain engagement and strength.

4.3 Finite element analysis of the overall frame assembly

To further validate the overall structural rigidity and strength of the vertical seedling frame under full-load conditions, and to improve the representativeness of finite element verification, static FEA of the complete frame assembly was performed.

The full assembly model includes the main load-bearing frame, chain drive system, triangular tray supports, seedling trays, anti-tilt mechanism, and anti-torsion device, with dimensions fully consistent with the prototype design in Section 3.1. Tetrahedral elements were used for meshing (Figure 12), with local mesh refinement for key stressed components. The material properties are consistent with Table 3, and the allowable stress is calculated with a safety factor of 1.5, consistent with the previous component verification.

A uniform load of 300 Pa (consistent with Section 5.1) was applied to all seedling trays, along with gravity load and 1.2 kN chain pre-tension, to simulate the worst-case full-load operating conditions. The bottom surface of the frame base was fully fixed, and frictional contact was set for all moving fit pairs of the assembly.

The total deformation cloud diagram of the assembly is shown in Figure 13. The maximum total deformation of the structure is 0.275 51 mm, which occurs at the midpoint of the middle-layer tray beam, far below the allowable deflection limit for agricultural machinery steel structures. The equivalent (von Mises) stress cloud diagram is shown in Figure 14. The maximum stress of the overall structure is 52.388 MPa, which is far below the allowable stress of Q235 steel (156.67 MPa) for the main frame and 45Cr steel (236.67 MPa) for key components.

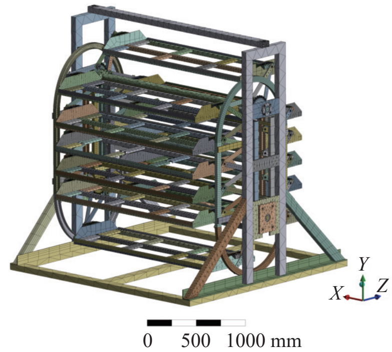

Figure 12 Mesh model of the overall vertical seedling frame assembly

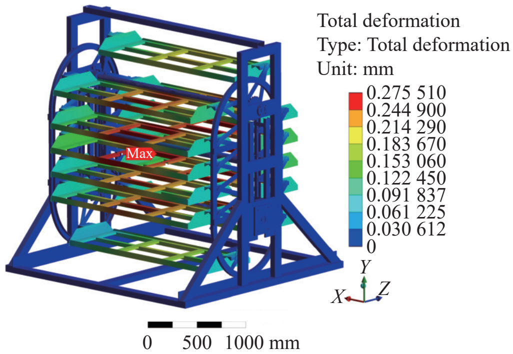

Figure 13 Total deformation cloud diagram of the overall frame assembly

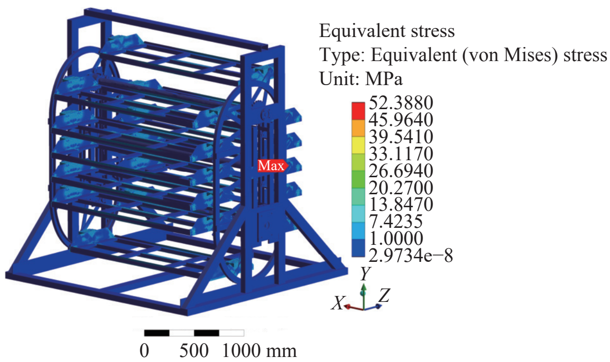

Figure 14 Equivalent (von Mises) stress cloud diagram of the overall frame assembly

These results confirm that the overall frame assembly meets the rigidity and strength requirements under full-load operating conditions. This analysis complements the component-level verification in Sections 5.1 and 5.2, and fully validates the structural safety and long-term operational stability of the designed system.

5 Prototype testing

5.1 Digital prototype simulation

A digital mock-up (DMU) of the rack and tray motion was constructed in CAD software. A representative seedling model (150 mm height) was placed on a tray, and the entire motion cycle was simulated. Clearances among seedlings, trays, and frame were checked throughout stepping and sprocket turnarounds (Figure 15). The minimum distances found were: seedling-to-frame 144.0 mm, tray-to-seedling 62.1 mm, and tray-to-tray 118.5 mm; no collisions occurred. These clearances exceed the typical 50 mm safety margin for nursery conveyors, confirming an adequate mechanical envelope.

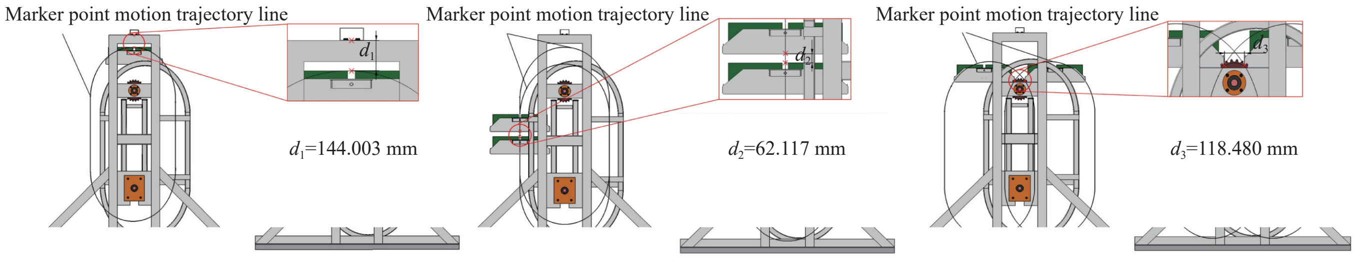

Figure 15 Clearance distances from the digital prototype (DMU): seedling↔frame, tray↔seedlings, and tray↔tray (mm)

5.2 Mechanical prototype testing (no-load and loaded)

A full-scale physical prototype (Figure 16) was fabricated. No-load tests showed smooth operation with the motor driving the chains and advancing trays as designed. Loaded tests (with seedling trays) also ran smoothly. Under typical seedling loads, the prototype advanced trays without jamming, tilting, or collisions. In particular, no instability was observed in any trial, validating the four-point conveying system's effectiveness. These results confirm that the mechanical design is stable and collision-free during real operation, as intended.

Figure 16 Physical prototype

5.3 LED lighting/DLI control verification

The DLI-based lighting control system was validated by measuring delivered light levels against targets. In tests, the system dynamically adjusted LED flux to achieve the set DLI values. The control loop successfully maintained the delivered DLI within its intended range each 24 h period. In practice, supplemental LED lighting was activated when actual DLI fell below the lower bound, and dimmed when exceeding the upper bound. Thus, the real-time lighting strategy performed as designed, ensuring each tier receives the uniform daily photon dose required for optimal growth.

5.4 Quantitative analyses and calculation checks

Data were checked for normality (Shapiro-Wilk) and homoscedasticity (Levene). One-way Analysis of Variance (ANOVA) (α=0.05) with Fisher's Least Significant Difference (LSD) post-hoc was used to compare treatments (n=3). Results are reported as mean ±SD; different letters denote significant differences at α=0.05. This procedure underlies the lettering in Table 5 and the error bars in the corresponding figures.

Table 5 Data comparison of various indicators

Indicator	Flat_mean	Flat_SD	Frame_ mean	Frame_SD	p_value_ or_letters	Units
Coverage rate	98	1	98	1	ns	%
Plant height	10.54	3.92	6.61	2.05	*a*/*b*	cm
Stem diameter	1.78	0.19	1.73	0.21	ns	mm

Note: Different letters (a/b) indicate significant differences at α=0.05 based on Fisher's LSD; ns, not significant.

A greenhouse comparison assessed the vertical frame against a traditional flat bench using identical trays and rice variety. Trays were randomly assigned, with n=3 replicates per treatment. Seedling coverage (%), plant height, stem diameter, and root length were measured at the 3-leaf stage. The daily light targets were identical; the vertical system achieved each DLI via closed-loop control (Section 3.1), whereas the flat bench used a fixed photoperiod schedule.

The number of effective seedlings N (at the three-leaf-one-heart stage) and the floor footprint S (m²) were used to compute land-use efficiency:

$$P = \frac{N}{S}[\text{seedlings/m}^2] \tag{6}$$

To compare treatments, a relative space-efficiency index was defined as:

$$\Delta P(\%) = 100\% \times \frac{P_{\text{frame}}}{P_{\text{flat}}} \tag{7}$$

where, ΔP>100% indicates the frame outperforms the flat bench. Here, N denotes the number of effective seedlings at the evaluation stage (same standard for both treatments), and S denotes the floor-projection area exclusively occupied by the treatment (shared aisles proportionally allocated).

Using Equation (6), the relative space-efficiency index was ΔP=119.29%, i.e., ≈19.29% higher space-use efficiency for the frame compared with the flat bench, without compromising seedling establishment or stem thickness.

Seedling coverage was 98%±1% in both treatments, with no significant difference (ns); stem diameter also showed no significant difference (ns), whereas plant height in the frame treatment was significantly lower than in the flat treatment (p<0.05; a/b), indicating a more compact phenotype.

6 Conclusions

This study developed a compact vertical rice seedling frame tailored for cold-region cultivation. The design integrates a triangular-truss tray support with a four-point conveying mechanism and anti-tilt/torsion features, ensuring trays move steadily along a fixed path. An adaptive LED lighting system based on daily light integral (DLI) dynamically adjusts supplemental light to meet seedlings' growth needs. Finite-element analysis and digital simulation confirmed that key structural components (frame, beams, tray) satisfy strength and stiffness requirements and that the conveyor path is collision-free. A physical prototype operated smoothly with no tipping or jams, validating the mechanical stability. In greenhouse trials, the system raised land-use efficiency to ΔP=119.29% (≈19.29% higher than flat beds), while maintaining high seedling coverage and uniform growth. These results demonstrate the proposed system's advantages for high-density seedling production. The approach is extensible to other transplantable crops (e.g. vegetables), offering significant potential for advancing automated nursery production in challenging climates.

Acknowledgements

This work was supported by the Project of Laboratory of Advanced Agricultural Sciences (Grant No. ZY04JD05-011).

[References]

[1] Shamshiri R R, Kalantari F, Ting K C, Thorp K R, Hameed I A, Weltzien C, et al. Advances in greenhouse automation and controlled environment agriculture: A transition to plant factories and urban agriculture. Int J Agric & Biol Eng, 2018; 11(1): 1–22.

[2] Ma C, Wang D Y, Hu Z Q, Li Z. Considerations of constructing quality, health and safety management system for agricultural products sold via e-commerce. Int J Agric & Biol Eng, 2018; 11(1): 31–39.

[3] Wicharuck S, Khongdee N, Syahputra W N H, Yalangkan P, Chaichana C. Vertical farming for lettuce production in limited space: A case study in Northern Thailand. PeerJ, 2024; 12: e17085.

[4] Warner R, Wu B S, MacPherson S, Lefsrud M. How the distribution of photon delivery impacts crops in indoor plant environments: A review. Sustainability, 2023; 15(6): 4645.

[5] Gatkal N R, Nalawade S M, Sahni R K, Bhanage G B. Review of IoT and electronics-enabled smart agriculture. Int J Agric & Biol Eng, 2024; 17(5): 1–14.

[6] Warrier K, Rajendiran M, Kannan S K, Pillai R R. Design and development of automated vertical farming setup. Handbook of Smart Materials, Technologies, and Devices: Applications of Industry 4.0. Cham: Springer International Publishing, 2022: 891–926.

[7] Kyratzis A C, Pallides A, Katsiotis A. Development of a precision sensor-based multi-layer vertical farm. Agronomy, 2022; 12(8): 1774.

[8] Yi S J, Zhang G, Li Y F, Li B H, Luo L S, Wang P. Design and experiment of a fully automatic plate lifting machine for rice hard disk seedling cultivation. Agriculture, 2023; 13(10): 1929.

[9] Niu G L, Wang G L, Li B B, Song C N, Xiao W W, Zhou H B. Design of rice factory three-dimensional carpet raising seedlings system engineering. IERI Procedia, 2014; 8: 93–100.

[10] Liu N, Ji F, Xu L J, He D X. Effects of LED light quality on the growth of pepper seedling in plant factory. Int J Agric & Biol Eng, 2019; 12(5): 44–50.

[11] Li M Y, Jin X, Ji J T, Li P G, Du X W. Design and experiment of intelligent sorting and transplanting system for healthy vegetable seedlings. Int J Agric & Biol Eng, 2021; 14(4): 208–216.

[12] Chen S L, Liu A L, Tang F, Hou P, Lu Y L, Yuan P. Review of environmental control strategies and models for greenhouse microclimate. Sensors, 2025; 25(5): 1388.

[13] Faust J E, Logan J. Daily light integral: A research review and high-resolution maps of the United States. HortScience, 2018; 53(9): 1250–1257.

[14] Dou H J, Niu G H, Gu M M, Masabni J G. Responses of sweet basil to different daily light integrals in photosynthesis, morphology, yield, and nutritional quality. HortScience, 2018; 53(3): 496–502.

[15] Elkins C, van Iersel M W. Longer photoperiods with the same daily light integral improve growth of rudbeckia seedlings in a greenhouse. HortScience, 2020; 55(10): 1676–1682.

[16] Elkins C, van Iersel M W. Longer photoperiods with the same daily light integral increase daily electron transport through photosystem II in lettuce. Plants, 2020; 9(9): 1172.

[17] Yan Z N, Cao X X, Bing L X, Lin D, Cheng F, Wang K Y, et al. Assessment of the growth and quality of pepper seedlings under the combinations of daily light integral and nitrogen concentration. Horticulture, Environment, and Biotechnology, 2025; 66(2): 331–346.

[18] Gavhane K P, Hasan M, Singh D K, Kumar S N, Sahoo R N. Determination of optimal daily light integral (DLI) for indoor cultivation of iceberg lettuce in an indigenous vertical hydroponic system. Scientific Reports, 2023; 13(1): 10923.

[19] Kusuma P, Pattison P M, Bugbee B. From physics to fixtures to food: current and potential LED efficacy. Horticulture Research, 2020; 7: 56.

[20] Gallegos-Cedillo V M, Nájera C, Gruda N S, Signore A, Gallegos J, Rodríguez R, et al. An in-depth analysis of sustainable practices in vegetable seedling nurseries: A review. Scientia Horticulturae, 2024; 334: 113342.

[21] Zou J, Liu W B, Wang D W, Luo S P, Yang S J, Ding X T, et al. Comparative study of artificial-light plant factories and greenhouse seedlings of SAOPOLO tomato. PLoS One, 2025; 20(3): e0314808.

[22] Yuan X, Hu J, Marcelis L F M, Heuvelink E, Peng J, Yang X, et al. Advanced technologies in plant factories: exploring current and future economic and environmental benefits in urban horticulture. Horticulture Research, 2025; 12(5): uhaf024.

[23] He R, Ju J, Liu K Z, Song J L, Zhang S C, Zhang M G, et al. Technology of plant factory for vegetable crop speed breeding. Frontiers in Plant Science, 2024; 15: 1414860.

[24] Mun H S, Lagua E B, Hong S K, Ryu S B, Sharifuzzaman M, Hasan M K, et al. Energy-efficient technologies and strategies for feasible and sustainable plant factory systems. Sustainability, 2025; 17(7): 3259.

[25] Hwang I, Kim D, Yoon S, Kim J H, Son J E. Estimation of supplemental lighting requirements of greenhouse crops based on canopy light interception using 3D plant models and ray-tracing simulation. ISHS Acta Horticulturae, 2023; 1377: 291–298.

[26] Zhou B, Miao H, Guan C, Ji X, Wang X C. Design and test of seedling-picking mechanism of fully automatic transplanting machine. Applied Sciences, 2024; 14(20): 9235.

[27] Yang J J, Zhou M L, Yin D Q, Yin J J. Design and development of rice pot-seedling transplanting machinery based on a non-circular gear mechanism. Applied Sciences, 2024; 14(3): 1027.

[28] Zhang L, Huang T, Zhang Q Q, Wei S W, Contreras V H E, Peng J, et al. Plant factory technology as a tool for improving vegetable quality: lettuce as an example. Vegetable Research, 2024; 4: e017.

[29] Wang C L, Luo L F. Application of smart technology and equipment in horticulture. Horticulturae, 2024; 10(7): 676.

[30] Yang R, Yang H, Ji F, He D. Enhancing the photon yield of hydroponic lettuce through stage-wise optimization of the daily light integral in an LED plant factory. Agronomy, 2024; 14(12): 2949.

[31] Alaviani S S, van Iersel M W, Velni J M. Optimal supplemental lighting control for an extended photoperiod in controlled environment agriculture. IFAC-PapersOnLine, 2022; 55(37): 639–644.

[32] Velasco M H. Enabling year-round cultivation in the Nordics-Agrivoltaics and adaptive LED lighting control of daily light integral. Agriculture, 2021; 11(12): 1255.

[33] Baghalian K, Ranasingha R. Vertical farming of hardy nursery stock: LED-driven propagation strategies compared with industry practice. Frontiers in Plant Science, 2026; 16: 1697104.